

Aspects of Lattice QCD Calculations of Transverse Momentum-Dependent Parton Distributions

M. Engelhardt^{a†}, B. Musch^b, T. Bhattacharya^c, J. R. Green^d, R. Gupta^c, P. Hägler^b, J. Negele^e, A. Pochinsky^e, A. Schäfer^b, S. Syritsyn^f and B. Yoon^c

^a*Department of Physics, New Mexico State University, Las Cruces, NM 88003, USA*

^b*Institut für Theoretische Physik, Universität Regensburg, 93040 Regensburg, Germany*

^c*Theoretical Division, Los Alamos National Laboratory, Los Alamos, NM 87545, USA*

^d*Institut für Kernphysik, Johannes Gutenberg-Universität Mainz, 55099 Mainz, Germany*

^e*Center for Theoretical Physics, Massachusetts Institute of Technology, Cambridge, MA 02139, USA*

^f*Theory Center, Thomas Jefferson National Accelerator Facility, Newport News, VA 23606, USA*

[†]*E-mail: engel@nmsu.edu*

Transverse momentum-dependent parton distributions (TMDs) can be formally defined in terms of hadronic matrix elements of quark bilocal operators containing staple-shaped gauge connections. A parametrization of the matrix elements in terms of invariant amplitudes serves to cast them in the Lorentz frame preferred for a lattice calculation. An ongoing program of evaluating TMD observables within Lattice QCD is reviewed, summarizing recent progress with respect to several challenges faced by such calculations. Results on the naively T-odd Sivers and Boer-Mulders effects are presented.

QCD Evolution 2015 –QCDEV2015–

May 26-30, 2015

Jefferson Lab (JLAB), Newport News, Virginia, USA

*Speaker.

1. Introduction

In the description of hadron structure, transverse momentum-dependent parton distribution functions [1] (TMDs) play a role complementary to generalized parton distributions (GPDs). Whereas GPDs encode information about the transverse spatial distribution of partons, TMDs contain information about the transverse momentum distribution of partons. As detailed further below, the definition of TMDs involves a number of subtleties not encountered in the case of GPDs, which also must be taken into account in formulating corresponding Lattice QCD calculational schemes. Cast in a Lorentz frame in which the hadron of mass m_h propagates with a large momentum in 3-direction, $P^+ \equiv (P^0 + P^3)/\sqrt{2} \gg m_h$, the quark momentum components scale such that TMDs are principally functions $f(x, k_T)$ of the quark longitudinal momentum fraction $x = k^+/P^+$ and the quark transverse momentum vector k_T , with the dependence on the component $k^- \equiv (k^0 - k^3)/\sqrt{2} \ll m_h$ becoming ignorable in this limit. $f(x, k_T)$ will thus be regarded as having been integrated over k^- .

Experimentally, TMDs manifest themselves in angular asymmetries observed in processes such as semi-inclusive deep inelastic scattering (SIDIS) and the Drell-Yan (DY) process. Corresponding signatures have emerged at COMPASS, HERMES and JLab [2–4], and that has motivated targeting a significant part of the physics program at future experiments in this direction, e.g., at the upgraded JLab 12 GeV facility and at the proposed electron-ion collider (EIC). To relate the experimental signature to the hadron structure encoded in TMDs, a suitable factorization framework is required. One possible such framework which is particularly well-suited for connecting phenomenology to a Lattice QCD calculation has been advanced in [5–8]. Factorization in the TMD context is considerably more involved than standard collinear factorization, with the resulting TMDs in general being process-dependent, via initial and/or final state interactions between the struck quark and the hadron remnant.

In the following, a review of an ongoing program of evaluating TMD observables within Lattice QCD is presented. In laying out the scheme by which the phenomenological definition of TMDs can be cast into a form amenable to lattice evaluation, challenges faced by such calculations are highlighted. Recent progress in meeting those challenges is reviewed, using selected TMD observables as examples, in particular time-reversal odd (T-odd) observables such as the Sivers and Boer-Mulders shifts. A detailed account of some aspects of this work was presented in [9, 10].

2. Definition of TMD observables

The fundamental correlator defining TMDs is of the form

$$\Phi^{[\Gamma]}(x, k_T, P, S, \dots) = \int \frac{d^2 b_T}{(2\pi)^2} \int \frac{d(b \cdot P)}{(2\pi)P^+} \exp(ix(b \cdot P) - ib_T \cdot k_T) \frac{\tilde{\Phi}_{\text{unsubtr.}}^{[\Gamma]}(b, P, S, \dots)}{\mathcal{S}(b^2, \dots)} \Big|_{b^+=0} \quad (2.1)$$

with

$$\tilde{\Phi}_{\text{unsubtr.}}^{[\Gamma]}(b, P, S, \dots) \equiv \frac{1}{2} \langle P, S | \bar{q}(0) \Gamma \mathcal{U}[0, \dots, b] q(b) | P, S \rangle \quad (2.2)$$

where S denotes the hadron spin and Γ an arbitrary γ -matrix structure. Heuristically, the Fourier-transformed bilocal quark bilinear operator counts quarks of momentum k , with Γ controlling the

spinor components involved. However, gauge invariance additionally enforces the introduction of the gauge connection \mathcal{U} , the precise path of which is not specified at this point; its choice will be guided by the physical process under consideration. In turn, the presence of \mathcal{U} introduces divergences additional to the wave function renormalizations of the quark operators (this is indicated by the subscript “unsubtr.”); these divergences accordingly are compensated by the additional “soft factor” $\widetilde{\mathcal{S}}$. Here, $\widetilde{\mathcal{S}}$ does not need to be specified in detail, since only appropriate ratios in which the soft factors cancel will ultimately be considered. Finally, $\Phi^{[\Gamma]}(x, k_T, P, S, \dots)$ is, as noted further above, a function only of the three quark momentum components contained in x and k_T , whereas the small component k^- is integrated over; thus, in its Fourier transform, the conjugate component b^+ is set to zero, as written in (2.1).

Decomposing the correlator $\Phi^{[\Gamma]}(x, k_T, P, S, \dots)$ into the relevant Lorentz structures yields the TMDs as coefficient functions. Quoting only the structures relevant for the following discussion,

$$\Phi^{[\gamma^+]} = f_1 - \left[\frac{\varepsilon_{ij} k_i S_j}{m_h} f_{1T}^\perp \right]_{\text{odd}} \quad (2.3)$$

$$\Phi^{[i\sigma^{i+}\gamma^s]} = S_i h_1 + \frac{(2k_i k_j - k_T^2 \delta_{ij}) S_j}{2m_h^2} h_{1T}^\perp + \frac{\Lambda k_i}{m_h} h_{1L}^\perp + \left[\frac{\varepsilon_{ij} k_j}{m_h} h_1^\perp \right]_{\text{odd}} \quad (2.4)$$

where Λ denotes the hadron helicity (i.e., $S^+ = \Lambda P^+ / m_h$, $S^- = -\Lambda m_h / 2P^+$) for hadrons with spin. In particular, the two TMDs f_{1T}^\perp and h_1^\perp are odd under time reversal, and can only arise if a mechanism is operative which breaks time-reversal invariance. The former TMD, characterizing the unpolarized distribution of quarks in a transversely polarized hadron, is the Sivers function, whereas the latter TMD, characterizing the distribution of transversely polarized quarks in an unpolarized hadron, is the Boer-Mulders function.

The above definition needs to be embedded into a factorization framework which connects TMDs to a physical process alongside other elements of the process, such as the hard, perturbative vertex and possibly a fragmentation function describing the hadronization of the struck quark. For selected processes, including the SIDIS and DY processes, factorization arguments have indeed been constructed, one possible approach having been advanced, e.g., in [5–8]. A crucial aspect in the description of, e.g., SIDIS is the inclusion of final-state gluon exchanges between the struck quark and the hadron remnant. These final state effects break time-reversal invariance and thus lead to nontrivial T-odd TMDs. At a formal level, a resummation of these gluon exchanges in the spirit of an eikonal approximation yields a Wilson line approximately following the trajectory of the struck quark, close to the light cone. This motivates a specific choice for the gauge connection between the quark operators in (2.2). Namely, parallel Wilson lines are attached to both of the quark operators, extending to large distances along a direction v close to the light cone; at the far end, these lines are connected by a Wilson line in the b direction to maintain gauge invariance. The result is a staple-shaped connection $\mathcal{U}[0, \eta v, \eta v + b, b]$, where the path links the positions in the argument of \mathcal{U} with straight line segments, and η parametrizes the length of the staple. Formally, thus, it is the introduction of the additional vector v which breaks the symmetry under time reversal and makes nonvanishing Sivers and Boer-Mulders effects possible.

At first sight, the most convenient choice for the staple direction v would seem to be a light-like vector. However, beyond tree level, this introduces rapidity divergences which require regularization. One advantageous way to accomplish this is to take v slightly off the light cone into the

space-like region [5, 6], with perturbative evolution equations governing the approach to the light cone [7]. Within this scheme, common TMDs describe both SIDIS and DY, except that in the DY process, it is initial state interactions which play a crucial role; correspondingly, the staple direction v is inverted and the T-odd TMDs acquire a minus sign. A scheme in which v (along with the quark operator separation b) is generically space-like is also attractive from the point of view of Lattice QCD, as discussed further below. It will thus constitute the starting point for the development of the lattice calculation. A useful parameter characterizing how close v is to the light cone is the Collins-Soper evolution parameter

$$\hat{\zeta} = v \cdot P / (|v| |P|), \quad (2.5)$$

in terms of which the light cone is approached for $\hat{\zeta} \rightarrow \infty$.

The correlator (2.2) can be decomposed in terms of invariant amplitudes \tilde{A}_{iB} . Listing only the components relevant for the Siverson and Boer-Mulders effects,

$$\frac{1}{2P^+} \tilde{\Phi}_{\text{unsubtr.}}^{[\gamma^+]} = \tilde{A}_{2B} + im_h \varepsilon_{ij} b_j S_i \tilde{A}_{12B} \quad (2.6)$$

$$\frac{1}{2P^+} \tilde{\Phi}_{\text{unsubtr.}}^{[i\sigma^{i+}\gamma^5]} = im_h \varepsilon_{ij} b_j \tilde{A}_{4B} - S_i \tilde{A}_{9B} - im_h \Lambda b_i \tilde{A}_{10B} + m_h [(b \cdot P)\Lambda - m_h (b_T \cdot S_T)] b_i \tilde{A}_{11B}. \quad (2.7)$$

These amplitudes are useful in that they can be evaluated in any desired Lorentz frame, including the frame which is particularly suited for the lattice calculation. On the other hand, in view of (2.3)-(2.4), they are closely related to Fourier-transformed TMDs. Performing the appropriate algebra, and quoting only the components necessary for defining the Siverson and Boer-Mulders shifts below¹,

$$\tilde{f}_1^{[1(0)]}(b_T^2, \hat{\zeta}, \dots, \eta v \cdot P) = 2\tilde{A}_{2B}(-b_T^2, b \cdot P = 0, \hat{\zeta}, \eta v \cdot P) / \tilde{\mathcal{F}}(b^2, \dots) \quad (2.8)$$

$$\tilde{f}_{1T}^{\perp[1(1)]}(b_T^2, \hat{\zeta}, \dots, \eta v \cdot P) = -2\tilde{A}_{12B}(-b_T^2, b \cdot P = 0, \hat{\zeta}, \eta v \cdot P) / \tilde{\mathcal{F}}(b^2, \dots) \quad (2.9)$$

$$\tilde{h}_1^{\perp[1(1)]}(b_T^2, \hat{\zeta}, \dots, \eta v \cdot P) = 2\tilde{A}_{4B}(-b_T^2, b \cdot P = 0, \hat{\zeta}, \eta v \cdot P) / \tilde{\mathcal{F}}(b^2, \dots) \quad (2.10)$$

where the generic Fourier-transformed TMD² is defined as [11]

$$\tilde{f}^{[1(n)]}(b_T^2, \dots) = n! \left(-\frac{2}{m_h^2} \partial_{b_T^2} \right)^n \int_{-1}^1 dx \int d^2 k_T e^{ib_T \cdot k_T} f(x, k_T^2, \dots). \quad (2.11)$$

The $b_T \rightarrow 0$ limit formally yields k_T -moments of TMDs. However, this limit contains additional singularities, which one can view as being regulated by a finite b_T . Here, results will only be given at finite b_T . Note the presence of the soft factors $\tilde{\mathcal{F}}$ on the right-hand sides of (2.8)-(2.10). One can construct observables in which the soft factors cancel by normalizing the (Fourier-transformed) Siverson and Boer-Mulders functions (2.9) and (2.10) by the unpolarized TMD (2.8), which essentially counts the number of valence quarks. Thus, one defines the ‘‘generalized Siverson shift’’

$$\langle k_y \rangle_{TU}(b_T^2, \dots) \equiv m_h \frac{\tilde{f}_{1T}^{\perp[1(1)]}(b_T^2, \dots)}{\tilde{f}_1^{[1(0)]}(b_T^2, \dots)} = -m_h \frac{\tilde{A}_{12B}(-b_T^2, 0, \hat{\zeta}, \eta v \cdot P)}{\tilde{A}_{2B}(-b_T^2, 0, \hat{\zeta}, \eta v \cdot P)} \quad (2.12)$$

which is the regularized, finite- b_T generalization of the ‘‘Siverson shift’’

$$m_h \frac{\tilde{f}_{1T}^{\perp[1(1)]}(0, \dots)}{\tilde{f}_1^{[1(0)]}(0, \dots)} = \frac{\int dx \int d^2 k_T k_y \Phi^{[\gamma^+]}(x, k_T, S_T = (1, 0))}{\int dx \int d^2 k_T \Phi^{[\gamma^+]}(x, k_T, S_T = (1, 0))}, \quad (2.13)$$

¹The treatment can be readily expanded to nonzero $b \cdot P$, providing access to the x -dependence of TMDs.

²Advantages of analyzing experimental data in terms of Fourier-transformed TMDs have been discussed in [12].

which, in view of the right-hand side, formally represents the average transverse momentum of unpolarized (“ U ”) quarks orthogonal to the transverse (“ T ”) spin of the hadron, normalized to the corresponding number of valence quarks. In the interpretation of (2.13), it should be noted that the numerator sums over the contributions from quarks and antiquarks, whereas the denominator contains the difference between quark and antiquark contributions, thus giving the number of valence quarks. Analogously, one can also extract the generalized Boer-Mulders shift

$$\langle k_y \rangle_{UT}(b_T^2, \dots) = m_h \frac{\tilde{A}_{4B}(-b_T^2, 0, \hat{\zeta}, \eta v \cdot P)}{\tilde{A}_{2B}(-b_T^2, 0, \hat{\zeta}, \eta v \cdot P)}. \quad (2.14)$$

Besides the soft factors, the ratios (2.12) and (2.14) also cancel multiplicative wave function renormalization constants attached to the quark operators in (2.2). It should be emphasized that the construction presented up to this point has been developed within continuum QCD; transferring it verbatim to Lattice QCD constitutes a working assumption which ultimately requires further consideration. In particular, the breaking of space-time symmetries engendered by the lattice discretization may imply changes to the purely multiplicative nature of the soft factors and renormalization constants exhibited above, and thus invalidate the cancellations invoked in the construction of the ratios (2.12) and (2.14). Pending a foundational investigation of these issues within the lattice formulation, empirical insight into possible renormalization effects can be obtained by studying the stability of TMD ratios such as (2.12) and (2.14) under substantial changes of the lattice discretization. This constitutes one of the topics addressed in the presentation of numerical results below.

3. Lattice calculational scheme

The formal framework laid out above provides all the necessary elements for a Lattice QCD evaluation of generalized shifts such as (2.12) and (2.14). One calculates hadron matrix elements of the type (2.2) and then decomposes them into invariant amplitudes, as given in (2.6)-(2.7). For this to be possible, it is crucial to work in a scheme where the four-vectors b and v are generically space-like, for the following reason: By employing a Euclidean time coordinate to project out hadron ground states via Euclidean time evolution, Lattice QCD cannot straightforwardly accommodate operators containing Minkowski time separations. The operator of which one takes matrix elements thus has to be defined at a single time. Only if both b and v are space-like is there no obstacle to boosting the problem to a Lorentz frame in which b and v are purely spatial, and evaluating $\tilde{\Phi}_{\text{unsubtr.}}^{[\Gamma]}$ in that frame. The results extracted for the invariant amplitudes \tilde{A}_{iB} are then immediately valid also in the original frame in which (2.2) was initially defined, thus completing the determination of quantities of the type (2.12) and (2.14).

Since, in a numerical lattice calculation, the staple extent η necessarily remains finite, two extrapolations must be performed from the generated data, namely, the one to infinite staple length, $\eta \rightarrow \infty$, and the extrapolation of the staple direction towards the light cone, $\hat{\zeta} \rightarrow \infty$. As discussed below, the former extrapolation is fairly straightforward. On the other hand, the extrapolation $\hat{\zeta} \rightarrow \infty$ constitutes a considerable challenge. Given that v is purely spatial in the Lorentz frame used for the lattice calculation, the accessible range of $\hat{\zeta}$ is determined by the available hadron spatial momenta P (in units of the hadron mass), cf. (2.5). The numerical signal achieved in lattice calculations rapidly deteriorates with rising hadron momentum, and thus only a very limited set

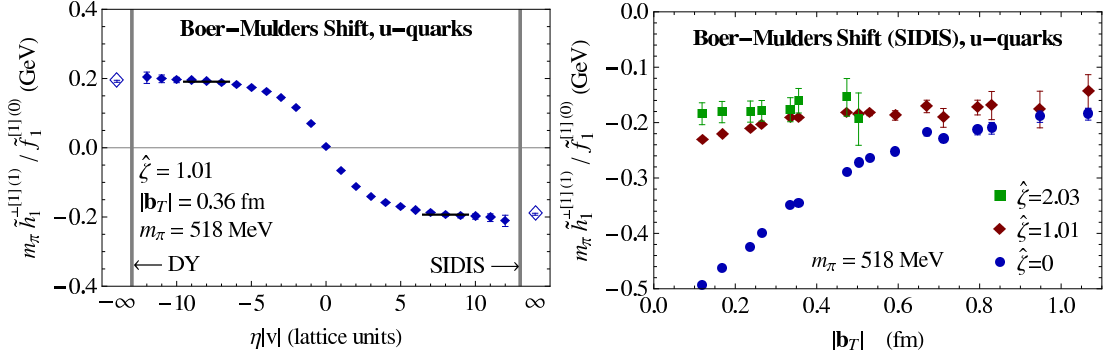


Figure 1: Generalized Boer-Mulders shift in a pion as a function of staple extent at fixed quark separation b_T and Collins-Soper evolution parameter $\hat{\zeta}$ (left); and as a function of b_T in the $\eta \rightarrow \infty$ SIDIS limit, at three different values of $\hat{\zeta}$ (right).

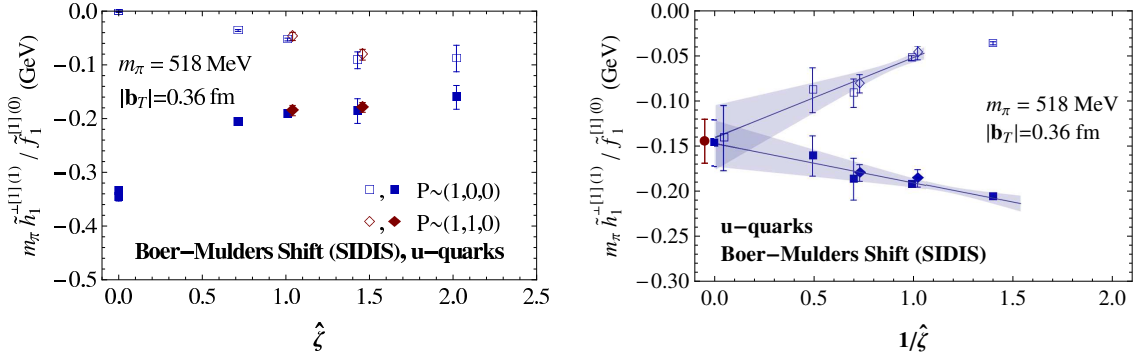


Figure 2: Generalized Boer-Mulders shift in a pion in the SIDIS limit as a function of Collins-Soper evolution parameter $\hat{\zeta}$ at fixed b_T (left); and as a function of $1/\hat{\zeta}$ together with fits using the form $c + d/\hat{\zeta}$ (right). Shown are both the full shift (filled symbols) as well as a partial contribution (open symbols), as detailed in the main text. Fit curves are for separate fits to the two cases; the extrapolated data point shown with a circle symbol results from a simultaneous fit to both.

of $\hat{\zeta}$ can be accessed. Data from a dedicated study of the Boer-Mulders shift in a pion [10] are discussed below to address this challenge; the lower mass of the pion compared to the nucleon facilitates reaching higher $\hat{\zeta}$ and makes a controlled extrapolation possible.

Finally, a general challenge faced by Lattice QCD calculations is reaching the physical pion mass. The computational expense of treating quark masses corresponding to the physical point has hitherto precluded the generation of lattice TMD data at that point. Instead, data are produced at artificially high pion masses. To also obtain preliminary insight into the pion mass dependence of TMD observables, data at differing pion masses are juxtaposed below.

4. Numerical results

Focusing first on the issue of $\hat{\zeta}$ -extrapolation, Figs. 1 and 2 display data for the generalized Boer-Mulders shift (2.14) in a pion [10], obtained in a mixed action scheme employing domain wall valence quarks on a MILC 2+1-flavor asqtad quark ensemble with a lattice spacing of $a = 0.12$ fm and a pion mass of $m_\pi = 518$ MeV. In the pion case, the isovector quark combination vanishes;

the shown data are for u -quarks alone, with the corresponding disconnected contributions omitted. Fig. 1 (left) exhibits results obtained at a given quark separation b_T and a given staple direction characterized by $\hat{\zeta}$, as a function of the staple extent. The T-odd behavior of the observable is evident, with $\eta \rightarrow \infty$ corresponding to the SIDIS limit, whereas $\eta \rightarrow -\infty$ yields the DY limit. The data level off to approach clearly identifiable plateaux as the staple length grows. The limiting SIDIS and DY values, represented by the open symbols, are extracted by imposing antisymmetry in η , allowing one to appropriately average the $\eta \rightarrow \pm\infty$ plateau values. Fig. 1 (right) summarizes the SIDIS limit values as a function of b_T for three different $\hat{\zeta}$. Remarkably, the b_T -dependence of the Boer-Mulders shift flattens as $\hat{\zeta}$ is increased, and the data for different $\hat{\zeta}$ approach each other at large b_T . It would be useful to understand this behavior in detail. Fig. 2 focuses on a particular value of b_T , displaying the $\hat{\zeta}$ -dependence of both the full Boer-Mulders shift as well as a certain partial contribution which vanishes at $\hat{\zeta} = 0$, but dominates the quantity at large $\hat{\zeta}$; comparison of the full Boer-Mulders shift with the partial contribution thus can give an indication of convergence towards the large $\hat{\zeta}$ limit. For further details, cf. [9, 10]. The partial contribution already furnishes roughly one half of the full shift at the highest $\hat{\zeta}$ reached, signaling that the calculation has covered a significant part of the evolution to large $\hat{\zeta}$. The right-hand panel of Fig. 2 shows an extrapolation to the large $\hat{\zeta}$ limit using the functional form $c + d/\hat{\zeta}$ (analogous fits using the form $c + d/\hat{\zeta}^2$ are seen to be inferior [10]). Given that the range of $\hat{\zeta}$ accessed numerically does not clearly overlap with the regime in which perturbative evolution equations become applicable, this form should be viewed as no more than a physically motivated ad hoc ansatz. The fits to the full and partial data converge to compatible values, agreeing also with a combined fit to both data sets. This buttresses confidence in the extrapolations and demonstrates that lattice calculations can achieve a signal for the Boer-Mulders shift of sufficient quality such that it survives taking the $\hat{\zeta} \rightarrow \infty$ limit.

Turning to the issue of the dependence of TMD ratios on the lattice discretization, which provides an empirical test of whether renormalization effects indeed cancel in such observables, Figs. 3 and 4 show representative results for the generalized Sivers shift (2.12) in the nucleon. Results for the isovector, $u - d$ quark combination are displayed; in this channel, couplings of the operator insertion to disconnected quark loops in the nucleon, which have not been evaluated, cancel. The figures juxtapose results obtained on a RBC/UKQCD 2+1-flavor domain wall fermion ensemble featuring a lattice spacing of $a = 0.084$ fm and a pion mass of $m_\pi = 297$ MeV with results obtained on a 2+1-flavor clover fermion ensemble provided by K. Orginos and collaborators in the Jefferson Lab lattice group; the latter has a lattice spacing of $a = 0.114$ fm and a pion mass of $m_\pi = 317$ MeV. The two ensembles thus have very similar pion masses, but differ substantially in the lattice discretization. The domain wall fermion ensemble not only features a considerably finer spacing, but also respects chiral symmetry to the largest extent possible, whereas the clover fermion ensemble strongly breaks the continuum symmetry. Fig. 3, analogously to Fig. 1 (right), shows the SIDIS limit results as a function of b_T at a given $\hat{\zeta}$, where the shaded area below $|b_T| = 2a$ indicates the region where the data may be significantly affected by finite lattice cutoff effects. Fig. 4, analogously to Fig. 2 (left), displays the dependence of the SIDIS limit results on the Collins-Soper evolution parameter $\hat{\zeta}$, with $|b_T|$ kept fixed. As in Fig. 2, both the full Sivers shift as well as a certain partial contribution are exhibited, cf. the comments in connection with that figure. The results for the Sivers shift obtained on the two ensembles in question are compatible, despite the considerable differences in terms of discretization scheme. This suggests that the renormalization

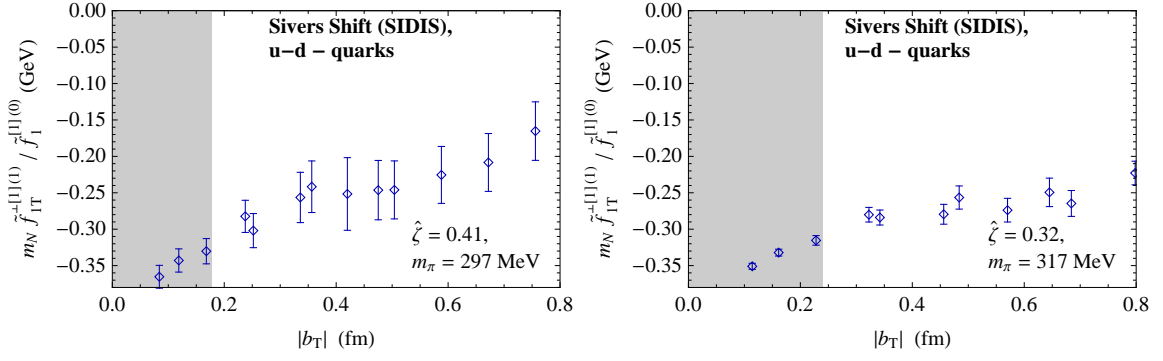


Figure 3: Generalized Sivers shift in a nucleon as a function of b_T in the $\eta \rightarrow \infty$ SIDIS limit, at a fixed $\hat{\zeta}$, in a fine lattice domain wall fermion calculation (left) and a coarse lattice clover fermion calculation (right), cf. main text for details.

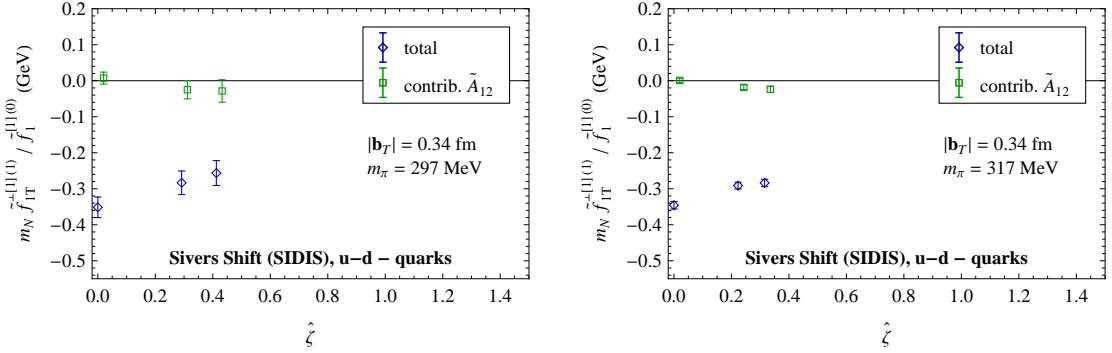


Figure 4: Generalized Sivers shift in a nucleon as a function of $\hat{\zeta}$ in the $\eta \rightarrow \infty$ SIDIS limit, at a fixed b_T , in a fine lattice domain wall fermion calculation (left) and a coarse lattice clover fermion calculation (right). Shown are both the full Sivers shift and a partial contribution, analogous to Fig. 2; cf. main text for details.

effects embodied in soft factors and wave function renormalization constants indeed cancel in TMD ratios also in the lattice formulation.

Finally, a preliminary indication of the pion mass dependence of TMD ratios is given by the juxtapositions in Figs. 5 and 6. These compare the domain wall fermion data for the Sivers shift in the nucleon at $m_\pi = 297$ MeV already displayed in Figs. 3 (left) and 4 (left) with corresponding nucleon Sivers shift data generated within the mixed action scheme already employed in obtaining the pion TMD results at $m_\pi = 518$ MeV in Figs. 1 and 2. Figs. 5 and 6 are analogous to Figs. 3 and 4, respectively, displaying the SIDIS limit data either as a function of b_T at a given $\hat{\zeta}$, or as a function of the Collins-Soper evolution parameter $\hat{\zeta}$ with $|b_T|$ kept fixed. Except for apparent discretization artefacts at small $|b_T|$ in Fig. 5, the results at the two pion masses are compatible; no significant variation of the Sivers shift is seen as the pion mass is changed. Recent preliminary analysis of data obtained on another RBC/UKQCD 2+1-flavor domain wall fermion ensemble at a pion mass of $m_\pi = 170$ MeV indicates that this behavior persists even as one approaches the physical point more closely [13], although it should be noted that these newer data still display sizeable statistical uncertainties.

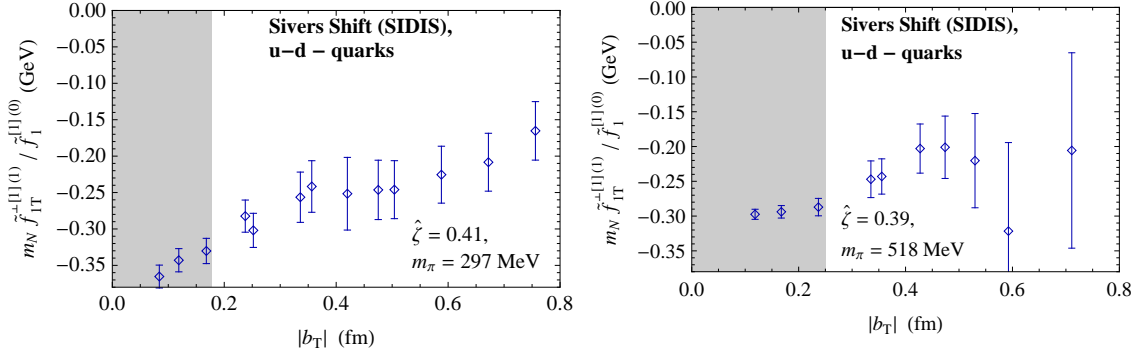


Figure 5: Generalized Sivers shift in a nucleon as a function of b_T in the $\eta \rightarrow \infty$ SIDIS limit, at a fixed $\hat{\zeta}$, in a domain wall fermion calculation at $m_\pi = 297$ MeV (left) and a mixed action calculation at $m_\pi = 518$ MeV (right), cf. main text for details.

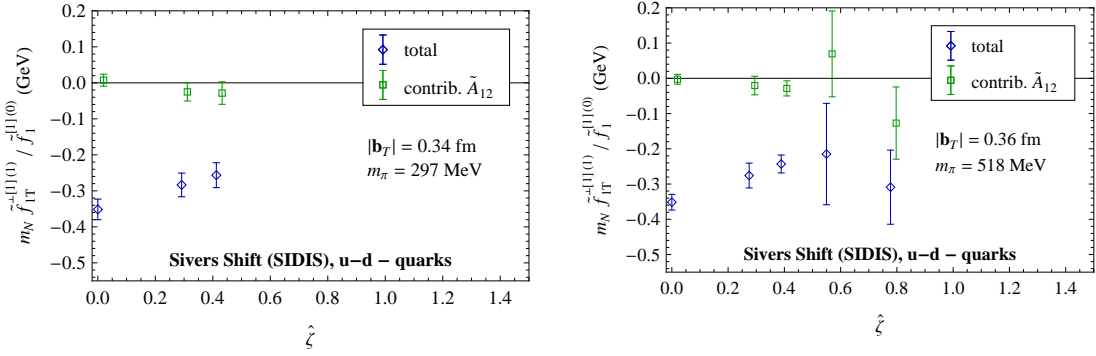


Figure 6: Generalized Sivers shift in a nucleon as a function of $\hat{\zeta}$ in the $\eta \rightarrow \infty$ SIDIS limit, at a fixed b_T , in a domain wall fermion calculation at $m_\pi = 297$ MeV (left) and a mixed action calculation at $m_\pi = 518$ MeV (right). Shown are both the full Sivers shift and a partial contribution, analogous to Fig. 2; cf. main text for further details.

5. Summary and outlook

TMDs can be formally defined in terms of hadronic matrix elements of quark bilocal operators containing staple-shaped gauge connections, which incorporate final/initial state effects in SIDIS/DY processes. Evaluating such matrix elements within Lattice QCD, one encounters several challenges. For one, to cancel multiplicative soft factors and renormalization constants, appropriate ratios of Fourier-transformed TMDs (“generalized shifts”, cf. (2.12) and (2.14)) are constructed. However, the breaking of space-time symmetries engendered by the lattice discretization may imply changes to the purely multiplicative nature of the soft factors and renormalization constants contained in the continuum definition; this possibility was addressed empirically by studying the universality of TMD ratios under changes of the discretization scheme. Secondly, the gauge connection staples are generically taken off the light cone to regularize rapidity divergences, with the Collins-Soper parameter $\hat{\zeta}$ controlling the approach to the light cone. A dedicated study of pion TMD ratios demonstrated that the attendant extrapolation in $\hat{\zeta}$ is feasible within Lattice QCD calculations. Thirdly, TMD calculations must ultimately approach the physical pion mass; the pion

mass dependence of TMD ratios has been explored, and no significant variations with pion mass have hitherto been observed. These results buttress the ongoing program of calculating TMD observables within Lattice QCD presented here. Beyond the TMD observables discussed above, the developed methods will also be useful to study generalized observables containing a nonzero momentum transfer in (2.2), which can be related to quark orbital angular momentum in the nucleon, since they provide mixed position and momentum information in the transverse plane.

Acknowledgements

Computations were performed using resources provided by the U.S. DOE Office of Science through the National Energy Research Scientific Computing Center (NERSC), a DOE Office of Science User Facility, under Contract No. DE-AC02-05CH11231, as well as through facilities of the USQCD Collaboration, employing the Chroma software suite [14]. The MILC and RBC/UKQCD collaborations are gratefully acknowledged for providing gauge ensembles analyzed in this work, as are K. Orginos (supported by DOE grant DE-FG02-04ER41302) and the Jefferson Lab lattice group (supported by DOE grant DE-AC05-06OR23177, under which Jefferson Science Associates, LLC, operates Jefferson Laboratory). Support by the Heisenberg-Fellowship program of the DFG (P.H.), SFB/TRR-55 (A.S.), the PRISMA Cluster of Excellence at the University of Mainz (J.G.), and the RIKEN Foreign Postdoctoral Researcher Program (BNL) as well as the Nathan Isgur Fellowship (JLab) (S.S.) is acknowledged. This work was furthermore supported by the U.S. DOE and the Office of Nuclear Physics through grants DE-FG02-96ER40965 (M.E.), DE-SC0011090 (J.N.) and DE-FC02-06ER41444 (A.P.). R.G., T.B. and B.Y. are supported by DOE grant DE-KA-1401020 and the LDRD program at LANL.

References

- [1] D. Boer, M. Diehl, R. Milner, R. Venugopalan, W. Vogelsang, *et al.*, arXiv:1108.1713.
- [2] M. Alekseev, *et al.*, COMPASS Collaboration, *Phys. Lett.* **B673** (2009) 127.
- [3] A. Airapetian, *et al.*, HERMES Collaboration, *Phys. Rev. Lett.* **103** (2009) 152002.
- [4] H. Avakian, *et al.*, CLAS Collaboration, *Phys. Rev. Lett.* **105** (2010) 262002.
- [5] S. M. Aybat and T. C. Rogers, *Phys. Rev.* **D 83** (2011) 114042.
- [6] J. C. Collins, *Foundations of Perturbative QCD* (Cambridge University Press, 2011).
- [7] S. M. Aybat, J. C. Collins, J.-W. Qiu and T. C. Rogers, *Phys. Rev.* **D 85** (2012) 034043.
- [8] J. C. Collins and T. C. Rogers, *Phys. Rev.* **D 87** (2013) 034018.
- [9] B. Musch, P. Hägler, M. Engelhardt, J. W. Negele and A. Schäfer, *Phys. Rev.* **D 85** (2012) 094510.
- [10] M. Engelhardt, P. Hägler, B. Musch, J. W. Negele and A. Schäfer, arXiv:1506.07826.
- [11] D. Boer, L. Gamberg, B. Musch and A. Prokudin, *JHEP* **1110** (2011) 021.
- [12] M. Aghasyan, *et al.*, *JHEP* **1503** (2015) 039.
- [13] M. Engelhardt, *et al.*, talk presented at the 33rd International Symposium on Lattice Field Theory (LATTICE 2015), Kobe, Japan, July 14-18, 2015, to appear in the proceedings.
- [14] R. G. Edwards and B. Joó, SciDAC Collaboration, *Nucl. Phys. Proc. Suppl.* **140** (2005) 832.